Appl Phys B (2010) 99: 173–179
DOI 10.1007/s00340-010-3902-4

Applied Physics B
Lasers and Optics

Effects of ambient pressure on Cu Kα X-ray radiation with millijoule and high-repetition-rate femtosecond laser

M. Hada · J. Matsuo

Received: 4 June 2009 / Revised version: 4 November 2009 / Published online: 6 February 2010

Abstract Hard Cu Kα X-ray radiation was generated with a millijoule and high-repetition-rate Ti: sapphire laser in air, helium or vacuum ($2.7–1.3 \times 10^4$ Pa) ambient. The characteristic X-ray was obtained by focusing the 0.06–1.46 mJ/pulse, 100 fs, 1 kHz repetition femtosecond laser onto a solid copper target to a spot 4.8 μm in diameter. The relationship between Kα X-ray conversion efficiency and atmospheric conditions was explained with a simple electron collision model that suggested that the electron mean free path is an important parameter in the generation of ultrafast pulsed X-rays in any ambient condition. We also demonstrated a high-intensity X-ray source working in helium at atmospheric pressure.

1 Introduction

When a high-intensity laser pulse is focused onto a metal target, ionization of the target material turns the surface into near-solid-density plasma. The absorption of the laser pulse into the surface material varies with the intensity of the laser-produced plasma. The intensity of the plasma generated on the laser focusing spot is a key parameter for the absorption of the laser pulse into the material and the generation of X-rays. The plasma intensity is calculated with the laser power of a single pulse, its pulse duration, wavelength and the diameter of focusing spot. Plasma intensity is expressed as $I\lambda^2$, where I and λ are the laser intensity and wavelength, respectively. In the range of lower plasma intensity, $I\lambda^2 < 1 \times 10^{15}$ W μm^2/cm^2, almost all of the absorbed laser energy transfers through collisional processes, such as inverse-bremsstrahlung [1–3]. In the plasma intensity range of 1×10^{15}–4×10^{16} W μm^2/cm^2, laser-produced plasmas are reportedly absorbed into the target via a more complicated collisionless process, such as resonant absorption [3–7]. In the higher plasma intensity range, $I\lambda^2 > 4 \times 10^{16}$ W μm^2/cm^2, the dominant absorption processes of laser-produced plasma are turned into vacuum heating [8]. Some other processes are important above plasma intensities of $I\lambda^2 > 1 \times 10^{17}$ W μm^2/cm^2, such as Raman heating or the two-dimensional effect [9, 10]. Hot electrons are created in the near surface region of the target with energy of 1–5 keV [11]. The hot electrons in the laser plasma interact with the incident laser pulse and are accelerated into the solid target. As the high-energy electrons penetrate into the target material, X-rays are generated via ionization of the target material, or bremsstrahlung. The pulse duration of these laser-produced X-rays is similar to the incident laser pulse, i.e., several hundred fs [12], because they occur when the hot electron is on the target surface. The laser-produced X-rays have gained much interest, as unique time-resolved X-ray diffraction (XRD) experiments demonstrate the atomic dynamics of chemical reactions, phase transition and coherent phonon vibrations [12–17]. For these time-resolved XRD experiments, a short-pulsed and high-intensity X-ray source of more than several 10^8 photons/sr/s is required.

Recently, a variety of femtosecond X-ray sources have been developed, in addition to the laser-produced plasmas. These include ultrafast hard X-rays produced by syn-

M. Hada (✉)
Department of Nuclear Engineering, Kyoto University, Gokasho, Uji, Kyoto 611-0011, Japan
e-mail: hadamasaki@nucleng.kyoto-u.ac.jp
Fax: +81-774-383978

J. Matsuo
Quantum Science and Engineering Center, Kyoto University, Gokasho, Uji, Kyoto 611-0011, Japan

chrotron and X-ray free electron laser (XFEL) [15, 18, 19]. However, the intensity or coherency of X-rays from synchrotrons or XFEL is quite high, and they are very expensive and require huge and complex facilities; moreover, because of usage limitations, the handling of a large number of samples is difficult. Laser-produced plasma X-ray sources are comparatively small in size and require only a lab-scale experimental facility. Laser-produced plasma X-ray sources consist of high-power, low-repetition-rate lasers of above 100 mJ and 10 Hz [20–23], and focusing such a high-power laser pulse requires a huge vacuum chamber. For time-resolved X-ray experiments, the Kα X-ray intensity obtained with this large-scale laser is quite high (10^9–10^{11} cps/sr with Cu Kα-X-ray conversion efficiency of 10^{-5}–10^{-4}), but the utilization of such an ultrafast pulsed X-ray source has been limited because of the complexity of the huge vacuum system and the difficulty in managing large, high-power lasers. Problems also exist in the use of complex vacuum systems, the limitation on target forms and debris from the target caused by laser ablation. Thin tape targets or wire targets have been used in vacuum chambers because of the space limitations. However, the lifetime of the target is quite short (from about a few hours to at most a few days). It is also difficult to control the position of the tape or wire target within a Rayleigh length of a few micrometers. Another problem is debris from the target. When the target surface in a vacuum is exposed to high-intensity laser plasma, the target materials are blown off by laser ablation and deposited onto the focusing lens, the windows of the vacuum chamber and other optical equipment. A thin polymer cover is used to remove the deposited debris. Ultrafast pulsed X-ray sources are required that are more compactly designed and easier to access. Recently, compact designed tabletop submillijoule to several millijoule femtosecond lasers have been used as short-pulsed X-ray sources under vacuum conditions. The intensities obtained from these compactly designed Kα X-ray sources in vacuum are 10^8–10^{10} cps/sr with conversion efficiency of 10^{-6}–10^{-5} [24–26]. This source with this compact laser achieved the X-ray intensity required for time-resolved XRD as well as reduction in the size of the femtosecond laser. Nevertheless, difficulties still remain in using a huge, complex vacuum chamber system, including problems of target form, target lifetime and debris from the target. Therefore, there is a need for a high-intensity X-ray source with a tabletop laser capable of operating in air.

The ultrafast X-ray source for atmospheric pressure (1.01×10^5 Pa) is a desirable tool for ultrafast time-resolved measurements. The total size of the X-ray source system could be reduced by eliminating the huge and complex vacuum system. It is also feasible to set a long-life and large-size target in air regardless of the vacuum chamber. The samples measured with time-resolved XRD can be placed close to the X-ray generating spot without a vacuum system, and this would enable using the generated X-ray more efficiency. Moreover, this vacuum-free X-ray system eliminates the debris problem. In atmospheric pressure, debris cannot reach the focusing lens, which is placed more than 10 mm away from the focusing spot. With the use of helium or other gas jet, debris can be collected easily with a filter. There have been a few reports of laser-produced plasma X-ray generation at atmospheric pressure in air [27]. However, the X-ray intensity or conversion efficiency in air was quite low and explaining the relationship between the X-ray intensity and the atmosphere near the target surface was difficult. In this paper, we demonstrate a laser-plasma-induced hard X-ray radiation with a tabletop femtosecond laser in various atmospheres, namely air, helium or vacuum (2.7–1.3×10^4 Pa). The relationship between Kα X-ray conversion efficiency and the ambient atmosphere near the target surface is explained with a simple electron collision model. This model suggests that the electron mean free path is the important parameter in laser-induced X-ray radiation. This result suggested the possibility of a vacuum-free high-intensity X-ray source in helium at atmospheric pressure.

2 Experimental

A schematic drawing of the experimental setup for ultrafast pulsed X-ray generation in various ambient atmospheres, i.e., air, helium or vacuum (2.7–1.3×10^4 Pa) is presented in Fig. 1. A mode-locked Ti: sapphire laser-generated optical pulses of about 100 fs duration with 800 nm wavelength, and the optical pulses were amplified at about 3.5 mJ/pulse through a regenerative amplifier (Spectra Physics Model Spitfire Pro XP) with a repetition rate of 1 kHz. The laser pulse profile was TEM_{00}. The optical pulse had a prepulse, which was generated in the regenerative amplifier of the laser system itself as leakage though the Pockels cell before the final pulse of the pulse train was switched off. The prepulse contrast to the main pulse was measured to be 8×10^{-4}, and the time separation between the prepulse and main pulse was 20 ns. The influence of a 10 ns prepulse plasma on X-ray generation can be negligible even if the prepulse generates preplasma on the target surface [24]. The *p*-polarized optical pulses were focused into a moving copper target with infrared achromatic lens ($f = 40$ mm) with a spot size of 4.8 μm. The duration of the laser pulse on the surface of the copper target was 100 fs and the energy of the optical pulse was 0.18–1.46 mJ. The moving copper target was placed in a vacuum chamber equipped with two leak valves used for varying the vacuum level. The surface position of the copper target was controlled within ±1 μm, which could be measured with a micrometer during motion. The ambient near the focus point in the Cu target

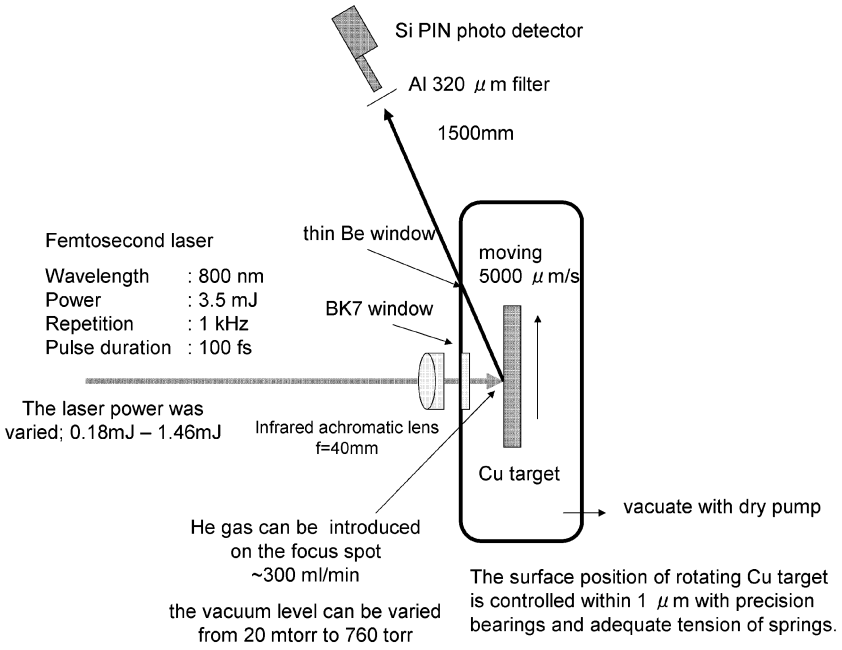

Fig. 1 Schematic drawing of the experimental setup for ultrafast pulsed X-ray generation in various ambient conditions

system could be varied between air, helium or vacuum (2.7–1.3×10^4 Pa). For samples immersed in helium ambient, the gas was introduced through a 1/4-inch gas nozzle and was blown onto the Cu target surface at a flowrate of 500 ml/min. For vacuum conditions, the chamber was evacuated with a dry pump with the leak valves closed (2.7 Pa) and with the leak valves opened (1.3×10^3 Pa/1.3×10^4 Pa).

The X-ray generated from focusing the laser pulse onto a copper target was measured with a p-intrinsic-n (PIN) Si photo detector (Amptek, XR-100CR),equipped with a 300 μm-thick, 7 mm^2 square silicon detector with detection efficiency of approximately 100% for 8 keV X-rays. The detector was sealed with a 25-μm-thick Be window in which an 8 keV X-ray penetrates without any loss. The signal from the detector was amplified with a spectroscopy amplifier (CANBERRA, 2022 Spectroscopy Amplifier) and was processed with a multichannel analyzer (SEIKO EG&G, TRUMP-MCA-2k). The detector was placed 1500 mm away from the focusing spot at an angle of 60°. Under vacuum conditions, the X-ray traveled 3 mm in a vacuum and 1497 mm in air. The attenuation value in ~1500 mm atmospheric air is 85% for Cu Kα X-ray. In He ambient or under vacuum conditions, a 320 μm thin aluminum filter was placed before the detector, and this reduces the intensity of Cy Kα X-rays by 1.72%. The long distance between the X-ray focusing spot, the detector and the Al filter allowed us to measure the X-ray photons as a Poisson distribution for single photon counting. A Si photo detector and a multichannel analyzer cannot detect two photons at once in a period on the order of 1 ms. If more than one photon is present at the same time, the total detected energy in the Si photo detector is doubled. For all conditions, it took 40 s to obtain each X-ray spectrum.

3 Results and discussion

Figure 2 shows the typical X-ray spectra generated at the focusing spot in vacuum and in air. The X-rays generated at the focusing spot went through 1500 mm in air and 320 μm Al filter (in helium or in a vacuum) for a single photon as measured with the Si PIN photo detector and multichannel analyzer. Thus, X-ray intensity was reduced depending on its energy. The energy spectra shown in Fig. 2 were calculated taking into account the reduction by the air layer and Al filter. The X-ray radiation from a *p*-polarized laser is regarded as an isotropic radiation hemisphere [28] and therefore, the X-ray spectra were computed into 2π. In the spectra presented in Fig. 2, a strong Cu Kα X-ray line (8.05 keV), Kβ X-ray line (8.91 keV) and a small part of bremsstrahlung X-ray were observed in the energy range of several keV. A rapid decline in Kα X-ray intensity occurred as the pressure increased above 1.3×10^4 Pa. Figure 3 shows the spectra of high-energy bremsstrahlung emission in the range of 10–14 keV in helium at atmospheric conditions at a plasma intensity of 4.0×10^{16} W μm^2/cm^2. The hot electron temperature could can be derived from Fig. 3. The Kα X-ray emission is found to be produced by a distribution function of hot electrons characterized by a temperature of ~3.4 keV, which corresponds well to the previously reported hot electron temperatures of 1–5 keV [11].

The Kα X-ray conversion efficiency ($\eta_{K\alpha}$) is defined as $\eta_{K\alpha} = nh\nu_{K\alpha}/E_{pulse}$, where n is the number of Kα X-ray photons generated per pulse, $h\nu_{K\alpha}$ is Kα X-ray energy, and E_{pulse} is the single pulse energy of incident laser. The plasma intensity was varied in the range 1.5×10^{15}–4.0×10^{16} W μm^2/cm^2 by varying the incident laser pulse

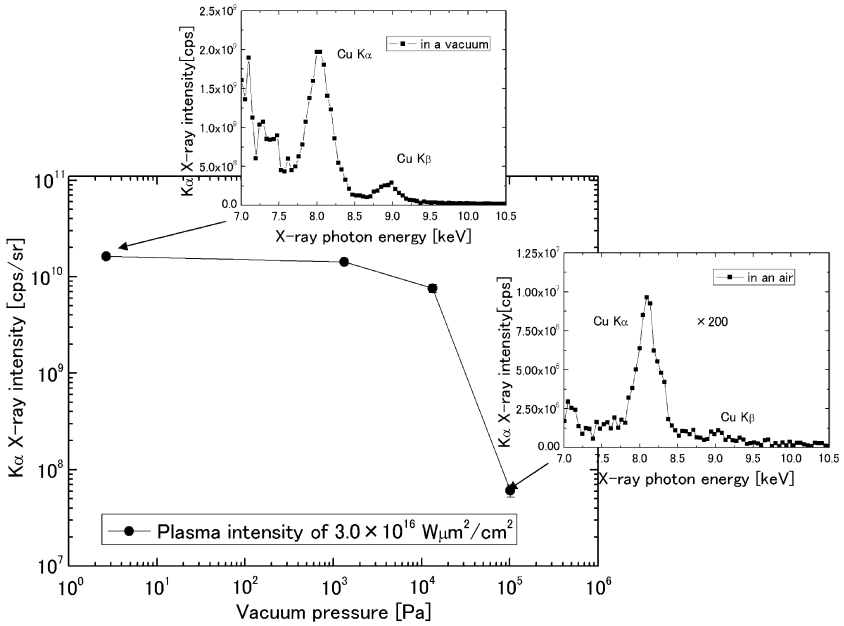

Fig. 2 Cu Kα X-ray intensity at a plasma power of 3.0×10^{16} W μm^2/cm^2 as a function of pressure. Two X-ray spectra are shown, in vacuum and in air

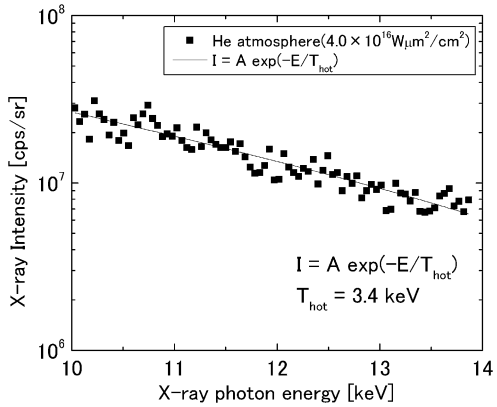

Fig. 3 Spectra of high-energy bremsstrahlung emission in the range 10–14 keV (in helium at atmospheric conditions; plasma intensity: 4.0×10^{16} W μm^2/cm^2). The X-ray intensity was fitted by a Maxwellian electron distribution; the hot electron temperature (T_{hot}) was found to be ~3.4 keV

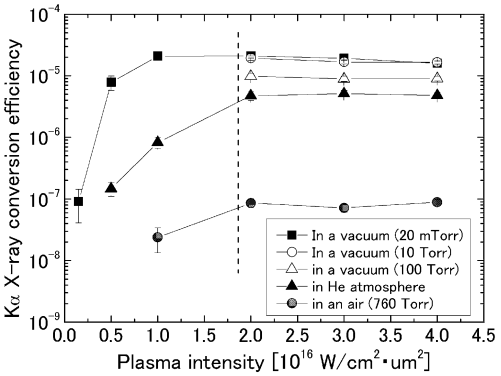

Fig. 4 Kα X-ray conversion efficiency, plotted as a function of plasma intensity under various conditions. *Symbols* are indicated in the *inset legend*. The *dashed line* shows the boundary of the intensity increasing region and the plateau

energy in the range 0.06–1.46 mJ/pulse (Fig. 4). At these plasma energies, the laser-produced plasma is absorbed into the target via a collisionless process such as resonant absorption. For all ambient conditions (vacuum (2.7–1.3×10^4 Pa), He and air at atmospheric pressure), the conversion efficiency increased as a power function in the plasma intensity range of 1.0–2.0×10^{16} W μm^2/cm^2, because more hot electrons were generated and their energy increased with plasma intensity; a plateau was reached at 2.0×10^{16} W μm^2/cm^2. These tendencies are similar to the experimental data obtained by other groups with high-repetition laser in a vacuum [25, 26]. The conversion efficiency in helium at atmospheric pressure was 5.0×10^{-6}, which was 30% of that at 2.7 Pa; in a vacuum of 1.3×10^4 Pa, the conversion efficiency was 50%–60% of that at 2.7 Pa. Overall, in vacuum conditions (2.7–1.3×10^4 Pa) and in a helium atmosphere, the conversion efficiency of the Kα X-ray was two orders of magnitude higher than in air.

The laser power lost in air or helium plasmas was quite low, below 10% and 1%, respectively. Moreover, the incident pulse duration of the laser was not extended in air or helium plasmas. The changes in pulse profile, in helium atmosphere, i.e., wavelength and pulse duration, were reported to be quite small for plasma intensities on the order of 1.0×10^{16} W μm^2/cm^2 [29–31]. This suggests that the effect of a reduction in plasma intensity or a breakdown in the ambient gases on the X-ray conversion efficiency in air or helium at atmospheric pressure is negligible. Some authors have indicated that the decrease in X-ray conversion efficiency in ambient atmosphere was caused by the defo-

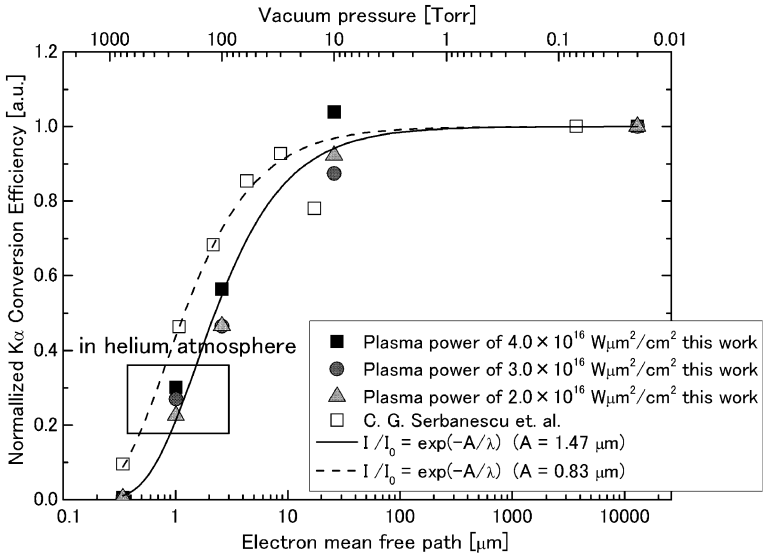

Fig. 5 Comparison between the normalized Kα X-ray conversion efficiency in this work and in Serbanescu et al. [35]. *Symbols* are indicated in the *inset legend*

cusing effect of the laser pulse in helium or in air [32–34]. Defocusing of the laser pulse on the focusing spot has occurred, but it is difficult to explain quantitatively the X-ray intensity reduction in ambient atmosphere only with the defocusing effect. The interactions between the generated electrons and the ambient atoms/molecules should be also considered in describing a proper model for the generation of laser-plasma-induced X-ray.

The Kα X-ray conversion efficiency in air or a vacuum of 1.3×10^3 Pa or 1.3×10^4 Pa was normalized with that in a vacuum of 2.7 Pa for the plasma intensities of 2.0–4.0×10^{16} W μm^2/cm^2. In Fig. 4, the Kα X-ray conversion efficiency normalized with that in a vacuum of 2.7 Pa was plotted as a function of pressure and electron mean free path. Regarding the electron generation and acceleration process, the target surface on the focusing spot changes into near-solid-density plasma by the incident laser pulse. The expansion region of the electrons in plasma is on the order of the incident pulse wavelength from the surface, within the time scale of several fs. After traveling through the expansion region, the electrons are accelerated by the incident laser pulse into the target. When there are atoms/molecules of ambient gas near the focusing spot, the electron can interact with these atoms/molecules before and while being accelerated. The electron traveling distance without interaction with the ambient gases is the electron mean free path in this atmosphere. The interaction cross-section between the electron and atoms/molecules is given by the simple electron collision model. The electron mean free path is expressed as the equation

$$\lambda = kT/(\pi r^2 p), \tag{1}$$

where λ is the electron mean free path in the ambient, k is the Boltzmann constant, r is the radius of the molecule and T and p are temperature (20°C) and pressure of the ambient gas. In air the pressure is 1.01×10^5 Pa and λ is 0.34 μm. At 1.3×10^4 Pa, 1.3×10^3 Pa and 2.7 Pa, the values of λ are 2.6 μm, 26 μm and 13 mm, respectively (Fig. 4, lower horizontal axis). In the simple electron collision model, electrons collide with the atoms/molecules in the ambient gas before or during their acceleration by the incident pulse. The electrons that collided with the ambient gas cannot reach the surface of the target material and therefore do not participate in the generation of Kα X-ray of the target materials. The energy of hot electrons in the plasma is in the range of 1–5 keV, and ions of the target materials in the plasma also have almost the same energy. In the first several fs, the ions in the plasma do not have enough velocity and remain near the target surface. The number of electrons accelerated by the incident pulse decreases exponentially as the electrons move into the ambient atmosphere as a result of the interaction between electrons and atoms/molecules in the ambient atmosphere. The number of X-ray photons is proportional to the number of accelerated electrons that arrived near the target material surface. Thus, the X-ray intensity can be expressed by the equation

$$I = I_0 \exp(-A/\lambda), \tag{2}$$

where I_0 is the intensity of the generated X-ray on the target, I is the intensity of the measured X-ray in the atmosphere and A and λ are average traveling length and electron mean free path in the atmosphere. In Fig. 4, the solid line represents the modified form of (2), i.e.,

$$I/I_0 = \exp(-A/\lambda), \tag{3}$$

with $A = 1.47$ μm.

The normalized X-ray conversion efficiency was well fitted with the equation of the simple electron collision

model. At plasma energies of 2.0×10^{16}, 3.0×10^{16} and 4.0×10^{16} W μm^2/cm^2, the values of A were fitted as 1.76 ± 0.13, 1.67 ± 0.21 and 1.31 ± 0.13 μm, respectively. This means that the electrons in the plasma traveled 1–2 μm in the atmosphere before incidence with the target surface or with the near-solid-density plasma of the target materials. Figure 4 also shows the relationship between the normalized X-ray conversion efficiency and the electron mean free path reported by Serbanescu et al. [35] at a plasma intensity of 6.9×10^{16} W/cm^2, which also fit well with the equations of the simple electrons collision model. The value of A in atmosphere was 0.83 ± 0.11 μm (Fig. 4, dotted line). Regarding the helium ambient, λ was calculated to be 1.01 μm at 1.01×10^5 Pa in air. The normalized X-ray conversion efficiency in helium ambient could also be fitted successfully with the equations of the simple electron collision model (Fig. 4), meaning that (2) described the X-ray conversion efficiency regardless of the specific atoms/molecules in the atmosphere. The electron mean free path at atmospheric pressure is also suggested as an important parameter in generating ultrafast pulsed X-ray in any ambient at atmospheric pressure.

The electron traveling length in a specific atmosphere should vary with the focusing conditions and the plasma intensity on the focusing spot. Generally, the gradient of the electrical field increases with plasma intensity, and the focusing spot size and the Rayleigh length of the incident pulse on the spot vary with focusing optics. Above a plasma intensity of 2.0×10^{16} W μm^2/cm^2, the average electron traveling length in the atmosphere was 1–2 μm and the electron mean free path of helium at atmospheric pressure was 1.01 μm. The X-ray intensity in helium ambient at atmospheric pressure was calculated to be 20%–40% of its value in vacuum conditions. We also obtained an X-ray conversion efficiency of 5.0×10^{-6}, which was 30% of that at 2.7 Pa, suggesting that a high-intensity ultrafast pulsed Kα X-ray source in helium operating at 1.01×10^5 Pa can be realized without vacuum.

4 Conclusion

We demonstrated that a hard X-ray radiation with millijoule and high-repetition-rate Ti: sapphire laser was generated in various ambient and pressure conditions in air, helium or vacuum (2.7–1.3×10^4 Pa). Cu Kα X-ray radiation was obtained by focusing the 0.06–1.46 mJ/pulse, 100 fs and 1 kHz repetition femtosecond laser on a solid Cu target with a plasma intensity of 1.5×10^{15}–4.0×10^{16} W μm^2/cm^2. The normalized Kα X-ray conversion efficiency in various conditions indicated that the simple electron collision model could explain the relationship between the Kα X-ray conversion efficiency and the atmosphere near the target surface. In this model, it is suggested that the electron mean free path in the specific atmosphere and pressure is an important parameter in the generation of the ultrafast pulsed X-ray. The electron traveling length in ambient atmosphere was well fitted to 1–2 μm and the electron mean free path in helium atmospheric pressure was 1.01 μm. Therefore, with (2), it is also suggested that the 20%–40% intensity (compared with the vacuum condition) ultrafast pulsed Kα X-ray is generated even in a helium ambient at 1.01×10^5 Pa. A high-intensity ultrafast pulsed X-ray source was realized without a vacuum system. This X-ray source enables us to avoid difficulties and complexities such as the target form or debris problem and also provides us stable and long life ultrafast pulsed X-ray.

Acknowledgements This work is supported by Core Research for Evolutional Science and Technology (CREST) of the Japan Science and Technology Agency (JST). We would like to thank Dr. T. Aoki, Dr. T. Seki, Dr. S. Ninomiya, Dr. Y. Nakata, Mr. K. Ichiki and Mr. H. Yamada from Kyoto University for discussions regarding X-ray generation systems. We also would like to thank Dr. Rafael Manory of editassociates.com for help with preparing this material for publication.

References

1. R.M. More, Z. Zinamon, K.H. Warren, R. Falcone, M. Murnane, J. Phys. C 7 **49**, 43 (1988)
2. E.G. Gamaly, Laser Part. Beams **12**, 185 (1994)
3. P. Gibbon, E. Forster, Plasma Phys. Control. Fusion **38**, 769 (1996)
4. R. Fedosejevs, R. Ottmann, R. Sigel, G. Kühnle, S. Szatmari, F.P. Schafer, Phys. Rev. Lett. **64**, 1250 (1990)
5. D.F. Price, R.M. More, R.S. Walling, G. Guethlein, R.L. Shepherd, R.E. Stewart, W.E. White, Phys. Rev. Lett. **75**, 252 (1995)
6. D.W. Forslund, J.M. Kindel, K. Lee, Phys. Rev. Lett. **39**, 284 (1977)
7. K. Eidmann, J. Meyer-ter-Vehn, T. Schlegel, S. Huller, Phys. Rev. E **62**, 1202 (2000)
8. E.S. Weibel, Phys. Fluids **10**, 741 (1967)
9. S.C. Wilks, Phys. Fluids B **5**, 2603 (1993)
10. S.C. Wilks, W.L. Kruer, M. Tabak, A.B. Langdon, Phys. Rev. Lett. **69**, 1383 (1992)
11. W. Rozmus, V.T. Tikhonchuk, R. Cauble, Phys. Plasmas **3**, 360 (1996)
12. K.G. Nakamura, S. Ishii, S. Ishitsu, M. Shiokawa, H. Takahashi, K. Dharmalingam, J. Irisawa, Y. Hironaka, K. Ishioka, M. Kitajima, Appl. Phys. Lett. **93**, 061905 (2008)
13. C. Rose-Petruck, R. Jimenez, T. Guo, A. Cavalleri, C.W. Siders, F. Raksi, J.A. Squier, B.C. Walker, K.R. Wilson, C.P.J. Barty, Nature (London) **398**, 310 (1999)
14. K. Sokolowski-Tinten, C. Blome, J. Blums, A. Cavalleri, C. Dietrich, A. Tarasevitch, I. Uschmann, E. Forster, M. Kammler, M. Horn-von-Hoegen, D. von der Linde, Nature (London) **422**, 287 (2003)
15. A.M. Lindenberg, J. Larsson, K. Sokolowski-Tinten, K.J. Gaffney, C. Blome, O. Synnergren, J. Sheppard, C. Caleman, A.G. MacPhee, D. Weinstein, D.P. Lowney, T.K. Allison, T. Matthews, R.W. Falcone, A.L. Cavalieri, D.M. Fritz, S.H. Lee, P.H. Bucksbaum, D.A. Reis, J. Rudati, P.H. Fuoss, C.C. Kao, D.P. Siddons, R. Pahl, J. Als-Nielsen, S. Duesterer, R. Ischebeck, H. Schlarb, H.

Schulte-Schrepping, Th. Tschentscher, J. Schneider, D. von der Linde, O. Hignette, F. Sette, H.N. Chapman, R.W. Lee, T.N. Hansen, S. Techert, J.S. Wark, M. Bergh, G. Huldt, D. van der Spoel, N. Timneanu, J. Hajdu, R.A. Akre, E. Bong, P. Krejcik, J. Arthur, S. Brennan, K. Luening, J.B. Hastings, Science **308**, 392 (2005)
16. D.M. Fritz, D.A. Reis, B. Adams, R.A. Akre, J. Arthur, C. Blome, P.H. Bucksbaum, A.L. Cavalieri, S. Engemann, S. Fahy, R.W. Falcone, P.H. Fuoss, K.J. Gaffney, M.J. George, J. Hajdu, M.P. Hertlein, P.B. Hillyard, M. Horn-von Hoegen, M. Kammler, J. Kaspar, R. Kienberger, P. Krejcik, S.H. Lee, A.M. Lindenberg, B. McFarland, D. Meyer, T. Montagne, É.D. Murray, A.J. Nelson, M. Nicoul, R. Pahl, J. Rudati, H. Schlarb, D.P. Siddons, K. Sokolowski-Tinten, Th. Tschentscher, D. von der Linde, J.B. Hastings, Science **315**, 633 (2007)
17. K. Scokilowski-Tinten, D. von der Linde, J. Phys. Condens. Matter **16**, R1517 (2004)
18. J. Chew, P. Lucas, S. Webber (eds.) (IEEE, Piscataway, 2003), p. 423
19. R. Service, Science **298**, 1356 (2002)
20. M. Yoshida, Y. Fujimoto, Y. Hironaka, K.G. Nakamura, K. Kondo, M. Ohtani, H. Tsunemi, Appl. Phys. Lett. **73**, 2393 (1998)
21. E.C. Eder, G. Pretzler, E. Fill, K. Eidmann, A. Saemann, Appl. Phys. B **70**, 211 (2000)
22. E. Fill, J. Bayerl, R. Tommasini, Rev. Sci. Instrum. **73**, 2190 (2002)
23. C.W. Siders, A. Cavalleri, K. Sokolowski-Tinten, T. Guo, C. Toth, R. Jimenez, C. Rose-Petruck, M. Kammler, M. Horn von Hoegen, D. von der Linde, K.R. Wilson, C.P.J. Barty, SPIE Proc. **3776**, 302 (1999)
24. C.L. Rettig, W.M. Roquemore, J.R. Gord, Appl. Phys. B **93**, 365 (2008)
25. M. Hagedorn, J. Kutzner, G. Tsilimis, H. Zacharias, Appl. Phys. B **77**, 49 (2003)
26. C.G. Serbanescu, J.A. Chakera, R. Fedosejevs, Rev. Sci. Instrum. **78**, 103502 (2007)
27. N. Takeyasu, Y. Hirakawa, T. Imasaka, Rev. Sci. Instrum. **72**, 3940 (2001)
28. Y. Hironaka, K.G. Nakamura, K. Kondo, Appl. Phys. Lett. **77**, 4110 (2000)
29. W.M. Wood, C.W. Siders, M.C. Downer, Phys Rev. Lett. **67**, 3523 (1991)
30. B.M. Penetrante, J.N. Bardsley, W.M. Wood, C.W. Siders, M.C. Downer, J. Opt. Soc. Am. B **9**, 2032 (1992)
31. F.V. Hartemann, A.L. Troha, H.A. Baldis, A. Gupta, A.K. Kerman, E.C. Landahl, N.C. Luhmann Jr., J.R. van Meter, Astrophys. J. Suppl. Ser. **127**, 347 (2000)
32. T. Auguste, P. Monot, L.A. Lompre, G. Mainfray, C. Manus, Opt. Commun. **89**, 145 (1992)
33. Y.M. Li, J.N. Broughton, R. Fedosejevs, T. Tomie, Opt. Commun. **93**, 366 (1992)
34. D. Umstadter, Appl. Phys. **36**, R151 (2003)
35. C.G. Serbanescu, J. Santiago, R. Fedosejevs, Proc. SPIE **5196**, 344 (2004)